

Beware the recent past: a bias in spectral energy distribution modeling due to bursty star formation

P. Haskell¹*, S. Das¹, D. J. B. Smith¹, R. K. Cochrane^{2,3}, C. C. Hayward³ and D. Anglés-Alcázar^{4,3}

¹Centre for Astrophysics Research, University of Hertfordshire, College Lane, Hatfield AL10 9AB, UK

²Department of Astronomy, Columbia University, New York, NY 10027, USA

³Center for Computational Astrophysics, Flatiron Institute, 162 Fifth Avenue, New York, NY 10010, USA

⁴Department of Physics, University of Connecticut, 196 Auditorium Road, U-3046, Storrs, CT 06269-3046, USA

Accepted XXX. Received YYY; in original form ZZZ

ABSTRACT

We investigate how the recovery of galaxy star formation rates (SFRs) using energy-balance spectral energy distribution (SED) fitting codes depends on their recent star formation histories (SFHs). We use the MAGPHYS and PROSPECTOR codes to fit 6,706 synthetic spectral energy distributions (SEDs) of simulated massive galaxies at $1 < z < 8$ from the Feedback in Realistic Environments (FIRE) project. We identify a previously unknown systematic error in the MAGPHYS results due to bursty star formation: the SFR estimates of individual galaxies can differ from the true values by as much as 1 dex, at large statistical significance ($> 5\sigma$), depending on the details of their recent SFH. The SFRs inferred using PROSPECTOR do not exhibit this trend, likely because unlike MAGPHYS, PROSPECTOR uses non-parametric SFHs. We urge caution when using MAGPHYS, or other codes assuming parametric SFHs, to study galaxies where the average SFR may have changed significantly over the last ~ 100 Myr, such as those which have recently quenched their star formation or those experiencing an ongoing burst. This concern is especially relevant, for example, when fitting JWST observations of very high-redshift galaxies.

Key words: galaxies: fundamental parameters - methods: data analysis - galaxies: photometry

1 INTRODUCTION

Star formation rates (SFRs) and star formation histories (SFHs) are both of great importance to our understanding of galaxies. SFRs are critical since (along with their stellar mass) they enable us to put galaxies in their contemporary context relative to the evolving SFR–stellar mass relation (e.g. Noeske et al. 2007). SFHs encode the build-up of stellar mass in the Universe (Dye 2008), potentially yielding insight into the physical processes that drive galaxy evolution (e.g. Madau et al. 1996; Behroozi et al. 2013; Wang et al. 2022). SFRs and other galaxy properties are typically inferred for high-redshift galaxies by fitting a model spectral energy distribution (SED) to the available data, using whatever photometry is available. There are many freely-available SED fitting codes able to do this (as discussed by e.g. Walcher et al. 2011; Conroy 2013; Baes 2019).

SED models frequently differ in their approach and assumptions in important ways which potentially impact the fidelity of inferred galaxy properties (Hunt et al. 2019, Pacifici et al. 2023). For example, they may employ different stellar population synthesis models (e.g. Bruzual & Charlot 2003, Maraston 2005, Conroy et al. 2009; see also Baldwin et al. 2018), initial mass functions (IMFs; e.g. Salpeter 1955, Kroupa 2001, Chabrier 2003; see also Kroupa & Jerabkova 2019), dust models (e.g. Calzetti 1997, Charlot & Fall 2000, Draine & Li 2007, da Cunha et al. 2008) and SFH forms. These can be parametric or non-parametric; while the former typically use one of many simple functional forms to represent the SFH (e.g. Behroozi

et al. 2013; Simha et al. 2014; Carnall et al. 2019), the latter can be implemented e.g. by partitioning the history into time bins and allocating stellar mass to each bin from a chosen prior distribution as the observations allow (e.g. Leja et al. 2019).

Many SED fitters, including two of the most well-known codes – MAGPHYS (da Cunha et al. 2008, 2015) and PROSPECTOR (Leja et al. 2017) – assume equality (or *balance*) between the energy absorbed by dust from starlight at short wavelengths and that which is re-radiated in the far-infrared. Physically, this must be true for the total absorbed and re-radiated luminosities (i.e. integrating over solid angle), but strict equality should not hold for every line of sight due to the non-isotropic nature of dust attenuation. Recent observations of spatial offsets between the starlight and dust in high-redshift galaxies (e.g. Hodge et al. 2016; Rujopakarn et al. 2019; Cochrane et al. 2021) cast doubt on whether these codes are appropriate in such cases where there is the potential for a lack of energy balance along a particular line of sight, to the point that other fitters explicitly avoid this assumption (e.g. Liu 2020; Kokorev et al. 2021). However, in Haskell et al. (2023, hereafter H23), we showed that the performance of MAGPHYS is similar for galaxies with UV/FIR spatial offsets as it is for local galaxies (Hayward & Smith 2015), suggesting that energy-balance codes remain the gold standard for deriving the properties of distant galaxies from photometric surveys.

With myriad codes available, with different physics and underlying assumptions, it is critical to validate the performance of each method. As well as the works of this group, which have compared the physical properties inferred using energy-balance SED fitting with MAGPHYS to simulated galaxies for which the ‘ground truth’ prop-

* E-mail: ph18aa@herts.ac.uk

erties are known (Hayward & Smith 2015; Smith & Hayward 2015, 2018; H23), there is a large body of work by other authors aiming to understand how well SED fitting works in different ways (e.g. da Cunha et al. 2008, Lee et al. 2009, Noll et al. 2009, Wuyts et al. 2009, Lee 2010, Pforr et al. 2012, Simha et al. 2014, Mobasher et al. 2015, Hunt et al. 2019, Dudzevičiūtė et al. 2020, Lower et al. 2020, Pacifici et al. 2023, Best et al. 2023). Since validation tests are often accomplished by averaging over a large population of galaxies, there is always danger of ‘washing out’ important details or systematic effects that could impact our understanding of how well SED fitting methods work in real-Universe situations.

In this Letter we build on the analysis of H23 and run the PROSPECTOR SED fitting code on the same synthetic galaxy SEDs for which we already have MAGPHYS fits, focusing on how the fidelity of the inferred SFR depends on the recent (i.e. within the last 100 Myr) SFH. Galaxies experiencing rapid changes in SFR over short (\sim 10s–100s of Myr) timescales have been identified both observationally (e.g. Guo et al. 2016, Faisst et al. 2019, Broussard et al. 2022, Loosher et al. 2023) and in simulations (e.g. Sparre et al. 2017, Iyer et al. 2020, Flores Velázquez et al. 2021, Hopkins et al. 2023).

In the FIRE simulations, massive galaxies at high redshift and dwarfs at all redshifts exhibit very bursty SFHs, with short (\sim 10-Myr) bursts followed by temporarily quenched periods¹ lasting a few 100 Myr; see Sparre et al. (2017) for a detailed analysis and Hayward & Hopkins (2017) and Hopkins et al. (2023) for discussions of the physical origin of this behavior. They thus provide an excellent test data set for exploring the effects of bursty star formation on SED modeling inferences.²

We demonstrate that MAGPHYS results exhibit a systematic bias in the inferred SFR due to bursty star formation: the SFR is overestimated (underestimated) for simulated galaxies experiencing a burst (temporarily quenched period). We show that PROSPECTOR does not exhibit this bias, likely due to its use of non-parametric SFHs.

The remainder of this Letter is structured as follows. In Section 2 we outline the tools and methods used to create the observations and to fit the SEDs, while in Section 3 we present the results of the fitting, and in Section 4 discuss the implications. In Section 5 we make some concluding remarks. We adopt a standard cosmology with $H_0 = 70 \text{ km s}^{-1} \text{ Mpc}^{-1}$, $\Omega_M = 0.3$, and $\Omega_\Lambda = 0.7$.

2 METHOD

To provide the synthetic SEDs used for this test, we used four cosmological zoom-in simulations of massive high-redshift galaxies from the FIRE project.³ The halos were first presented in Feldmann et al. (2016). Subsequently, the halos were resimulated by Anglés-Alcázar et al. (2017) using the FIRE-2 code (Hopkins et al. 2018); we use

¹ We will use the shorthand ‘temp-quenched’ to refer to the periods of low-specific SFR in between bursts that are common in the FIRE simulations analysed here. The term ‘mini-quenched’ has been used by some authors, but given that ‘mini’ refers to size rather than temporal duration, we believe that ‘temp-quenched’ is more accurate. We use the term ‘starbursting’ to refer to simulated galaxies that are currently undergoing a burst, i.e. the 10 Myr-averaged SFR is greater than the 100 Myr-averaged value.

² Owing to the lack of AGN feedback in these simulations, none of the simulated galaxies are permanently quenched. However, because the bias depends on the shape of the SFH over the past 100 Myr, our conclusions should apply equally well to galaxies that are undergoing quenching and will remain quenched permanently, not only ‘temp-quenched’ galaxies.

³ <http://fire.northwestern.edu>

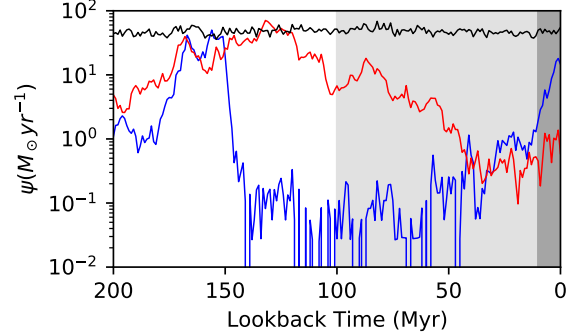


Figure 1. The recent SFHs (past 200 Myr) of three example simulated galaxies, showing a range of η values. The dark grey band encloses the previous 10 Myr, while the lighter band encloses the past 100 Myr; η is the ratio of the SFRs averaged over those two time periods. The black line shows an example of constant star formation with $\eta \approx 0$, while the red line shows a ‘temporarily quenched’ case ($\eta = -0.64$). The blue line shows an example simulated galaxy observed during a burst, where the star formation activity averaged over the previous 10 Myr has increased compared to the average over the previous 100 Myr (giving $\eta = 0.88$).

the simulations from that work. The simulations use the code GIZMO (Hopkins 2015),⁴ with hydrodynamics solved using the mesh-free Lagrangian Godunov ‘MFM’ method. The simulations include cooling and heating from a meta-galactic background and local stellar sources from $T \sim 10 - 10^{10}$ K; star formation in locally self-gravitating, dense, self-shielding molecular, Jeans-unstable gas; and stellar feedback from OB & AGB mass-loss, SNe Ia & II, and multi-wavelength photo-heating and radiation pressure, with inputs taken directly from stellar evolution models. The FIRE physics, source code, and all numerical parameters are *exactly* identical to those in Hopkins et al. (2018).

Snapshots of the halos’ central galaxies were taken from $1 < z < 8$ at intervals of 15 – 25 Myr. For each snapshot, we compute the true 10 Myr and 100 Myr-averaged SFRs, $\bar{\psi}_{10 \text{ Myr}}$ and $\bar{\psi}_{100 \text{ Myr}}$, respectively. Following Broussard et al. (2019), we quantify the recent star forming activity using the ‘burst indicator’ $\eta = \log_{10}(\bar{\psi}_{10 \text{ Myr}} / \bar{\psi}_{100 \text{ Myr}})$, such that

$$\eta \begin{cases} < 0, & \text{galaxy has reduced SFR within the last 10 Myr;} \\ \approx 0, & \text{galaxy has had a constant SFR over the last 100 Myr;} \\ > 0, & \text{galaxy has increased SFR in the last 10 Myr.} \end{cases}$$

Figure 1 shows three example SFHs of snapshots used in this study with $\eta \approx 0$ (black line), $\eta < 0$ (red line) and $\eta > 0$ (blue line).

Cochrane et al. (2019) calculated synthetic SEDs for these simulated galaxies using the radiative transfer code SKIRT.⁵ Each snapshot was ‘observed’ at 7 viewing angles spaced at 30° intervals, ranging from aligned with the angular momentum vector to anti-aligned. This resulted in 6,706 forward-modeled SEDs. See Cochrane et al. (2019, 2022, 2023b,a) and Parsotan et al. (2021) for further details about the SKIRT calculations and other applications of these and similar simulations/SEDs. We convolved these SEDs with the filter response curves for 18 photometric bands spanning observed-frame wavelengths $0.39 < \lambda/\mu\text{m} < 500$ (we refer the interested reader to H23 for further details) assuming a signal-to-noise ratio of 5 in

⁴ <http://www.tapir.caltech.edu/~phopkins/Site/GIZMO.html>

⁵ <http://www.skirt.ugent.be/>

every band (following [Smith & Hayward 2018](#)). We fit the synthetic SEDs using two SED fitting codes, MAGPHYS ([da Cunha et al. 2008](#), hereafter DC08) and PROSPECTOR ([Leja et al. 2017, 2019](#), [Johnson et al. 2021](#)), fixing the redshift to the true value (i.e. photometric redshift errors do not contribute to the bias demonstrated here). We use the high-redshift version of MAGPHYS ([da Cunha et al. 2015](#)) which builds model UV–FIR SEDs by linking a stellar library containing 50,000 pre-computed SFHs with those which satisfy the energy balance criterion among another pre-computed library of 25,000 [Charlot & Fall \(2000\)](#) dust models; see DC08 and H23 for detailed discussions. By calculating the χ^2 goodness-of-fit parameter between the observed photometry and every combination which satisfies the energy balance, MAGPHYS is able to marginalise over the prior distribution to estimate posterior probability distributions for each property in the model. MAGPHYS assumes an initial mass function (IMF) from [Chabrier \(2003\)](#), and stellar models from [Bruzual & Charlot \(2003\)](#) for metallicity between 0.02 and 2 times solar.

For the PROSPECTOR fits, we followed the process described in [Das et al., in preparation](#). PROSPECTOR uses the Flexible Stellar Populations Synthesis (FSPS; [Conroy et al. 2009](#)) code assuming a [Kroupa \(2001\)](#) IMF and solar metallicity. Dust attenuation is modelled using the two-component [Charlot & Fall \(2000\)](#) model and the [Kriek & Conroy \(2013\)](#) attenuation curve. The three-parameter [Draine & Li \(2007\)](#), hereafter DL07 dust emission templates are used to model the shape of the IR SED. The dynamic nested sampling library [Dynesty \(Speagle 2020\)](#) is used to estimate Bayesian posteriors and evidences.

For both fitters, we consider an SED fit to be acceptable if the best fit χ^2 is below the 99 per cent confidence limit taken from standard χ^2 tables with the degrees of freedom calculated following [Smith et al. \(2012\)](#), who calculated this only for MAGPHYS; here we assume that it applies equally well to the PROSPECTOR results, though this is perhaps unlikely to be true given the differences between the two sets of models). Throughout the subsequent analysis, we consider only those SEDs with satisfactory fits.

Based on these analyses, we obtained four sets of estimated galaxy properties for each snapshot. The MAGPHYS values assume a fixed parameterisation of the SFH based on an underlying continuous, delayed exponential model overlaid with random starbursts (as detailed in DC08). In addition, we have three sets of results from PROSPECTOR, assuming different SFH priors: ‘Dirichlet’, ‘continuity’, and ‘bursty continuity’. The Dirichlet prior assumes that the fractional specific star formation rate (sSFR) in each time bin follows a Dirichlet distribution, with a concentration parameter, α , that controls the shape of the SFH ([Leja et al. 2017, 2019](#)), and which we set to unity. The ‘continuity’ prior directly fits for $\Delta \log(\text{SFR})$ between neighbouring time bins using a Student’s t -distribution with scale factor $\sigma = 0.3$ and two degrees of freedom. This prior discourages abrupt changes in SFR between adjacent bins but remains flexible enough to fit both star-forming and quenched galaxies ([Leja et al. 2019](#); [Johnson et al. 2021](#)). Following [Tacchella et al. \(2022\)](#), we also consider the bursty continuity prior, which is a modified form of the continuity prior with $\sigma = 1$ and $\nu = 2$, shown to allow even greater degrees of variability in the shape of the SFH. For each of these priors, we adopt the following binning scheme: the first two and the last bins are kept the same for all sources, covering $0 < t_l < 10$ Myrs, $10 < t_l < 100$ Myrs, and $0.85t_z < t_l < t_z$, respectively. Here, t_z represents the age of the Universe at the object’s redshift, and t_l is the lookback time. The remaining time between 100 Myrs and $0.85t_z$ is evenly spaced in logarithmic time. The number of bins is chosen to ensure each bin has a width greater than $0.02 \log_{10}$ Gyrs. For the lowest redshift snapshots in our simulated data set, this corresponds to eight bins, while for the highest redshifts, it is five.

Table 1. SED fit success rate and typical SFR estimate fidelity, $\Delta \log_{10}(\psi)$, for the MAGPHYS and PROSPECTOR fits to our synthetic observations. For the three sets of PROSPECTOR fits, the different SFH priors are indicated.

Fitter/prior	% Fit success	$\Delta \log_{10}(\psi)$
MAGPHYS	83	-0.11 ± 0.06
PROSPECTOR- Bursty-continuity	91	-0.09 ± 0.24
PROSPECTOR- Dirichlet ($\alpha = 1$)	92	-0.30 ± 0.19
PROSPECTOR- Continuity	92	-0.12 ± 0.12

For this study we are considering the fidelity of the 100 Myr averaged SFR inferred from the SED fitting of both MAGPHYS and PROSPECTOR. Following H23, we quantify the fidelity of the recovery of SFR, using the residual in dex between the inferred value and the true value (from the simulation) for the SFR, specifically: $\Delta \log_{10} \psi = \log_{10}(\psi_{\text{inferred}}) - \log_{10}(\psi_{\text{true}})$.

3 RESULTS

Table 1 shows the fit success rate and the average SFR residual for each of the four runs. It is immediately apparent that PROSPECTOR is able to produce acceptable fits for a larger fraction of the snapshots (> 90 per cent fit success rate irrespective of the prior assumed) than MAGPHYS (83 per cent). This may reflect the effect that the MAGPHYS pre-computed libraries – coupled with the requirement that it consider only SFHs shorter than the age of the Universe at a given redshift – result in the priors becoming increasingly poorly-sampled at higher redshifts, and acceptable MAGPHYS fits increasingly hard to obtain at earlier epochs. Secondly, we note that the typical SFR uncertainties for the PROSPECTOR runs shown in Table 1 are significantly larger than those yielded by MAGPHYS, and we will return to this point below. These details notwithstanding, it is clear from Table 1 that there is no significant difference in the overall $\Delta \log_{10} \psi$ once the uncertainties are considered, meaning that both codes do a similarly acceptable job of recovering the true SFR on average.

We now investigate the fidelity of the MAGPHYS and PROSPECTOR SFR estimates as a function of the recent SFH. In Figure 2, we plot $\Delta \log(\psi)$ against η , with the MAGPHYS results shown in the left-hand panel, and the PROSPECTOR results for the bursty continuity prior plotted in the right-hand panel. The axes are chosen such that ‘starbursting’ snapshots appear to the right of each plot, and ‘temp-quenched’ ones are on the left. The values for individual SEDs are shown as blue points, with the red lines showing a running average of $\Delta \log_{10}(\psi)$ for 100 data points. The red areas enclose the 16th and 84th percentiles of the inferred SFR PDF using the same running average, while the grey shading encloses the 16th and 84th percentiles of the scatter within each corresponding subsample.

Two effects are immediately apparent. First of all, there is a systematic trend in the MAGPHYS SFRs, such that while they are typically overestimated by ~ 0.4 dex at $\eta > 0.5$ (the ‘starbursting’ snapshots), the converse is true at $\eta < -0.5$ (the ‘temp-quenched’ snapshots) where MAGPHYS typically underestimates the true SFRs by around 0.3 dex. This is clearly of concern, since we know that both ‘starbursting’ and ‘temp-quenched’ galaxies exist in the real Universe (e.g. [Guo et al. 2016](#); [Faisst et al. 2019](#); [Broussard et al. 2022](#); [Loosher et al. 2023](#)) and this effect could – left unchecked – result in a systematic error in the SFRs of galaxies that could be 1 dex in magnitude in the worst cases. Secondly, and underscoring the severity of the first issue, there is a clear tendency for the typical MAGPHYS uncertainties (shown as the red shading in the left panel) to underestimate the degree of scatter visible in the data points (grey shading). This effect becomes increasingly noticeable as $|\eta|$ increases.

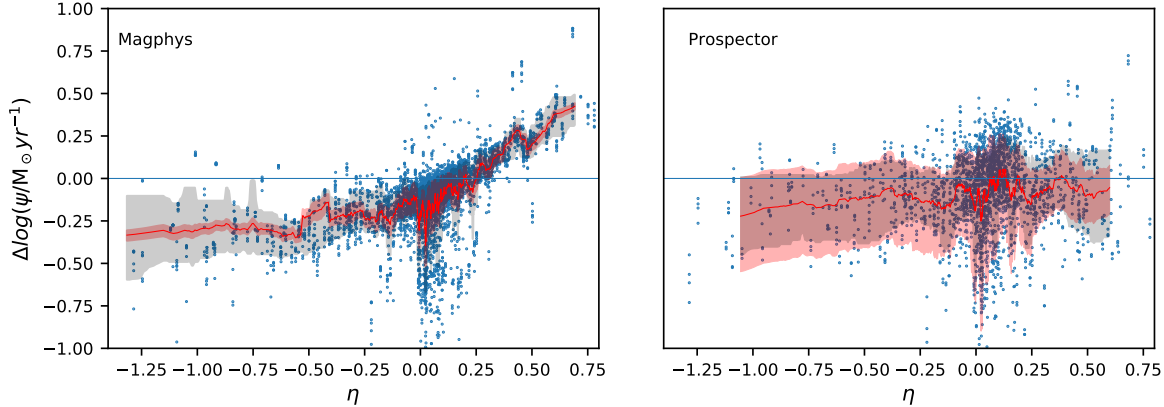


Figure 2. The LH panel shows the difference between the inferred and true SFRs averaged over the last 100 Myr, $\Delta \log_{10} \psi = \log_{10}(\psi_{\text{inferred}}) - \log_{10}(\psi_{\text{true}})$, as a function of the burst indicator $\eta \equiv \log_{10}(\bar{\psi}_{10 \text{ Myr}}/\psi_{100 \text{ Myr}})$. The RH panel show the same obtained using PROSPECTOR with the Bursty Continuity SFH prior (though similar results are obtained using different non-parametric priors). In both panels the red line shows the mean residual averaged over 100 data points with the red shaded area enclosing the averaged 16th and 84th percentile residuals from the PDF. The grey shaded area indicates the 16th and 84th percentiles of the scatter in $\Delta \log_{10} \psi$ within each averaged point, and the blue markers show values for individual SEDs. The MAGPHYS SFRs exhibit a systematic bias: the SFR tends to be underestimated for ‘temp-quenched’ galaxies and overestimated for galaxies that have experienced a burst within the past 10 Myr. This bias is not apparent in the PROSPECTOR results.

The equivalent PROSPECTOR plot shows the SFR recovery – $\Delta \log_{10}(\psi)$ – is approximately independent of η ; the same result is observed for the other PROSPECTOR priors with reasonable uncertainties at $\eta_{\text{true}} < 0.5$ (where ~ 90 per cent of the snapshots lie). At these η , the ~ 0.3 dex offset in the PROSPECTOR SFRs relative to the ground truth is similar to that returned by MAGPHYS at $\eta < -0.5$; however, in PROSPECTOR the deviation from zero is not statistically significant due to the more realistic error bars.

4 DISCUSSION

Fundamental to SED fitting codes’ abilities to recover the true properties of galaxies are (i) the wavelength sampling and (ii) the priors. The former issue is closely related to the extent of our ability to estimate η using SED fitting (since different wavelength regimes have different ‘response functions’ in terms of how the luminosity depends on the SFH; e.g. Kennicutt & Evans 2012; Sparre et al. 2017); we shall return to this topic in a future work (Das et al., *in preparation*). In this work we focus solely on our ability to recover 100 Myr-averaged SFRs using an example 18 bands of photometry similar to that used in Smith et al. (2021) for the LOFAR deep fields. This good wavelength sampling, in addition to the fact that we have not added noise to photometry, means that this test represents a best-case scenario: the bias that we have identified is fundamental, not due to noise or poor SED sampling, and thus cannot be addressed with ‘better data’.

In the MAGPHYS model, the priors are not under the control of the end user since it uses pre-computed SFH libraries. The high- z MAGPHYS SFHs assume a delayed exponential parametric form, with random bursts superposed in such a manner that during the previous 2 Gyr, 75 per cent of SFHs include a burst lasting between 30–300 Myr and forming between 0.1 and 100 times the stellar mass formed by the underlying distribution (da Cunha et al. 2015). The η distribution for the MAGPHYS high- z SFHs is shown by the blue histogram in Figure 3, overlaid with the distribution of values for the true SFHs of the simulated galaxies (hatched). It is clear that the libraries contain a significantly broader range of η values than the simulations, so the effective prior on η is not the source of the bias.

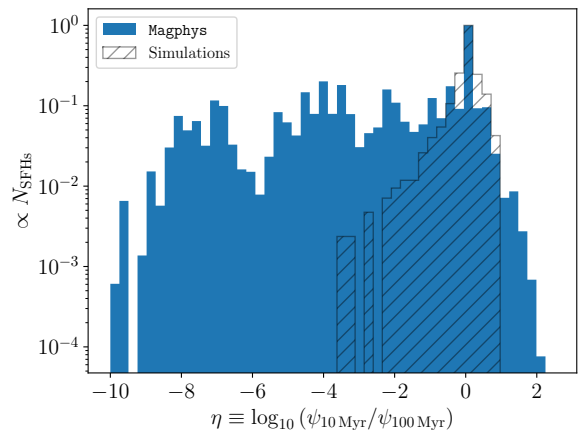


Figure 3. The distributions of η values for 50,000 SFHs in the MAGPHYS high- z libraries (in blue), overlaid with the ground truth values from the simulations (hatched) as indicated in the legend. Note the significantly larger x range in this plot relative to Figure 2, and the logarithmic axes.

In Section 3 we also noted a difference between the typical uncertainties on the MAGPHYS SFR estimates and the observed scatter, indicating that the uncertainties are increasingly underestimated as $|\eta|$ moves away from 0. Figure 3 shows that that SFHs with such η are far rarer in the MAGPHYS prior than those at $\eta \approx 0$, which may contribute to the underestimated error bars (which are up to a factor > 5 too small) in the SFRs of these sources.

PROSPECTOR offers a solution to this problem, likely as a result of the more flexible non-parametric SFH employed, and the improved ability to explore the parameter space using dynamic nested sampling. Even so, our results demonstrate that the choice of prior can impact the error estimates associated with PROSPECTOR SFRs for the most bursty galaxies (those with highest η), which is unsurprising given e.g. that the continuity prior tends to down-weight rapid changes in the SFHs.

5 CONCLUSIONS

We have used four cosmological zoom-in simulations spanning $1 < z < 8$, together with the radiative transfer code SKIRT, to generate 6,706 synthetic galaxy SEDs. We attempted to recover the true properties of synthetic observations based on these simulations using MAGPHYS and PROSPECTOR. Although there is little difference between the fidelity of SFR estimates inferred using the two codes when averaging over the whole sample, we find that the accuracy of the MAGPHYS-inferred SFR is strongly dependent on the recent SFH. This trend is sufficiently large that the MAGPHYS 100 Myr-averaged SFRs of individual galaxies could be overestimated (underestimated) by as much as 1 dex in the worst cases for galaxies experiencing starbursts (temporarily quenched periods). The trend is not evident in the 100 Myr SFRs from PROSPECTOR, which we speculate is due to the non-parametric SFHs assumed and possibly the dynamic nested sampling method used to better explore the parameter space. Given this bias, we caution against employing parametric SFHs when fitting the SEDs of observed galaxies that are likely to have bursty SFHs, such as high-redshift galaxies observed with JWST.

ACKNOWLEDGEMENTS

PH and DJBS would like to thank the Flatiron Institute for their hospitality. DJBS acknowledges support from the UK Science and Technology Facilities Council (STFC) under grant ST/V000624/1. This research has made use of NASA's Astrophysics Data System Bibliographic Services.

DATA AVAILABILITY

The data presented in this paper will be shared on reasonable request to the first author.

REFERENCES

Anglés-Alcázar D., Faucher-Giguère C.-A., Quataert E., Hopkins P. F., Feldmann R., Torrey P., Wetzel A., Kereš D., 2017, *MNRAS*, **472**, L109

Baes M., 2019, Proceedings of the International Astronomical Union, **15**, 26

Baldwin C., McDermid R. M., Kuntschner H., Maraston C., Conroy C., 2018, *MNRAS*, **473**, 4698

Behroozi P. S., Wechsler R. H., Conroy C., 2013, *ApJ*, **770**, 57

Best P. N., et al., 2023, *MNRAS*, **523**, 1729

Broussard A., et al., 2019, *ApJ*, **873**, 74

Broussard A., Gawiser E., Iyer K., 2022, *ApJ*, **939**, 35

Bruzual G., Charlot S., 2003, *MNRAS*, **344**, 1000

Calzetti D., 1997, *AJ*, **113**, 162

Carnall A. C., Leja J., Johnson B. D., McLure R. J., Dunlop J. S., Conroy C., 2019, *ApJ*, **873**, 44

Chabrier G., 2003, *PASP*, **115**, 763

Charlot S., Fall S. M., 2000, *ApJ*, **539**, 718

Cochrane R. K., et al., 2019, *MNRAS*, **488**, 1779

Cochrane R. K., et al., 2021, *MNRAS*, **503**, 2622

Cochrane R. K., Hayward C. C., Anglés-Alcázar D., 2022, *ApJ*, **939**, L27

Cochrane R. K., Anglés-Alcázar D., Cullen F., Hayward C. C., 2023a, *arXiv e-prints*, p. [arXiv:2310.08829](https://arxiv.org/abs/2310.08829)

Cochrane R. K., Hayward C. C., Anglés-Alcázar D., Somerville R. S., 2023b, *MNRAS*, **518**, 5522

Conroy C., 2013, *ARA&A*, **51**, 393

Conroy C., Gunn J. E., White M., 2009, *ApJ*, **699**, 486

da Cunha E., Charlot S., Elbaz D., 2008, *MNRAS*, **388**, 1595

da Cunha E., et al., 2015, *ApJ*, **806**, 110

Draine B. T., Li A., 2007, *ApJ*, **657**, 810

Dudzevičiūtė U., et al., 2020, *MNRAS*, **494**, 3828

Dye S., 2008, *MNRAS*, **389**, 1293

Faisst A. L., Capak P. L., Emami N., Tacchella S., Larson K. L., 2019, *ApJ*, **884**, 133

Feldmann R., Hopkins P. F., Quataert E., Faucher-Giguère C.-A., Kereš D., 2016, *MNRAS*, **458**, L14

Flores Velázquez J. A., et al., 2021, *MNRAS*, **501**, 4812

Guo Y., et al., 2016, *ApJ*, **833**, 37

Haskell P., Smith D. J. B., Cochrane R. K., Hayward C. C., Anglés-Alcázar D., 2023, *MNRAS*, **525**, 1535

Hayward C. C., Hopkins P. F., 2017, *MNRAS*, **465**, 1682

Hayward C. C., Smith D. J. B., 2015, *MNRAS*, **446**, 1512

Hodge J. A., et al., 2016, *ApJ*, **833**, 103

Hopkins P. F., 2015, *MNRAS*, **450**, 53

Hopkins P. F., et al., 2018, *MNRAS*, **480**, 800

Hopkins P. F., et al., 2023, *MNRAS*, **525**, 2241

Hunt L. K., et al., 2019, *A&A*, **621**, A51

Iyer K. G., et al., 2020, *MNRAS*, **498**, 430

Johnson B. D., Leja J., Conroy C., Speagle J. S., 2021, *ApJS*, **254**, 22

Kennicutt R. C., Evans N. J., 2012, *ARA&A*, **50**, 531

Kokorev V. I., et al., 2021, *ApJ*, **921**, 40

Kriek M., Conroy C., 2013, *ApJ*, **775**, L16

Kroupa P., 2001, *MNRAS*, **322**, 231

Kroupa P., Jerabkova T., 2019, *Nature Astronomy*, **3**, 482

Lee S.-K. J., 2010, PhD thesis, Johns Hopkins University, Maryland

Lee S.-K., Idzi R., Ferguson H. C., Somerville R. S., Wiklind T., Giavalisco M., 2009, *ApJS*, **184**, 100

Leja J., Johnson B. D., Conroy C., van Dokkum P. G., Byler N., 2017, *ApJ*, **837**, 170

Leja J., Carnall A. C., Johnson B. D., Conroy C., Speagle J. S., 2019, *ApJ*, **876**, 3

Liu D., 2020, michi2: SED and SLED fitting tool, Astrophysics Source Code Library, record ascl:2005.002 (ascl:2005.002)

Looser T. J., et al., 2023, *arXiv e-prints*, p. [arXiv:2306.02470](https://arxiv.org/abs/2306.02470)

Lower S., Narayanan D., Leja J., Johnson B. D., Conroy C., Davé R., 2020, *ApJ*, **904**, 33

Madau P., Ferguson H. C., Dickinson M. E., Giavalisco M., Steidel C. C., Fruchter A., 1996, *MNRAS*, **283**, 1388

Maraston C., 2005, *MNRAS*, **362**, 799

Mobasher B., et al., 2015, *ApJ*, **808**, 101

Noeske K. G., et al., 2007, *ApJ*, **660**, L43

Noll S., Burgarella D., Giovannoli E., Buat V., Marcillac D., Muñoz-Mateos J. C., 2009, *A&A*, **507**, 1793

Pacifici C., et al., 2023, *ApJ*, **944**, 141

Parsotan T., Cochrane R. K., Hayward C. C., Anglés-Alcázar D., Feldmann R., Faucher-Giguère C. A., Wellons S., Hopkins P. F., 2021, *MNRAS*, **501**, 1591

Pforr J., Maraston C., Tonini C., 2012, *MNRAS*, **422**, 3285

Rujopakarn W., et al., 2019, *ApJ*, **882**, 107

Salpeter E. E., 1955, *ApJ*, **121**, 161

Simha V., Weinberg D. H., Conroy C., Dave R., Fardal M., Katz N., Oppenheimer B. D., 2014, *arXiv e-prints*, p. [arXiv:1404.0402](https://arxiv.org/abs/1404.0402)

Smith D. J. B., Hayward C. C., 2015, *MNRAS*, **453**, 1597

Smith D. J. B., Hayward C. C., 2018, *MNRAS*, **476**, 1705

Smith D. J. B., et al., 2012, *MNRAS*, **427**, 703

Smith D. J. B., et al., 2021, *A&A*, **648**, A6

Sparre M., Hayward C. C., Feldmann R., Faucher-Giguère C.-A., Muratov A. L., Kereš D., Hopkins P. F., 2017, *MNRAS*, **466**, 88

Speagle J. S., 2020, *MNRAS*, **493**, 3132

Tacchella S., et al., 2022, *ApJ*, **927**, 170

Walcher J., Groves B., Budavári T., Dale D., 2011, *Ap&SS*, **331**, 1

Wang Y., et al., 2022, *MNRAS*, **515**, 3249

Wuyts S., Franx M., Cox T. J., Hernquist L., Hopkins P. F., Robertson B. E., van Dokkum P. G., 2009, *ApJ*, **696**, 348